Innovative Infrastructure Solutions (2025) 10:123
https://doi.org/10.1007/s41062-025-01901-6

TECHNICAL PAPER

Assessment of a base-isolated structure with semi-active low-cost viscous fluid dampers through real-time hybrid simulations

S. Vides[1] · B. Castillo[1] · A. Artunduaga[1] · J. Marulanda[1] · P. Thomson[1]

Received: 2 July 2024 / Accepted: 22 January 2025 / Published online: 5 March 2025

Abstract

The dynamic performance of low-rise buildings under dynamic loads presents significant challenges in structural engineering. Accurate evaluation methods are crucial for ensuring the safety and resilience of these structures, especially in seismic-prone areas. This study focuses on implementing Real-Time Hybrid Simulations (RTHS) for the assessment of structural control systems in low-rise buildings. The research integrates a numerical substructure, which models the dynamic characteristics of the building, with an experimental substructure that consists of physical devices such as base isolators, semi-active fluid viscous dampers, or hybrid control system. The RTHS method provides a sophisticated platform to evaluate the effectiveness of hybrid control systems under seismic excitations. The results demonstrated a marked improvement in predicting structural responses, with the proposed method achieving a 15.0% reduction in error compared to fixed structure. Additionally, the application of hybrid control systems showed a 25.0% increase in energy dissipation capacity compared to individual passive control. These findings contribute to the advancement of resilient design strategies, offering a quantitative framework for optimizing structural control systems in low-rise buildings.

Keywords Base isolation · Real-time hybrid simulation · Structural control systems · Viscous fluid dampers · Vibration mitigation strategies

Introduction

In recent years, the construction of resilient structures has been one of the main objectives in civil engineering. Resilient seismic design has become a fundamental approach in structural engineering to ensure the safety and functionality of buildings after seismic events. Structural control systems play a crucial role in this objective, enhancing the response of structures subjected to dynamic loads [1, 2]. One of the most efficient alternatives to achieve this is the use of structural control systems, whose objective is to manage the response of a structure subjected to dynamic loads by improving its properties through alternative mechanisms. These systems can be classified into four main categories: passive, active, semi-active, and hybrid, based on their energy requirements [3–5] and operating mechanisms [6]. Passive control systems do not require an external energy source; they generate forces that oppose the movement of the structure based solely on their mechanical properties and do not increase its total energy. On the other hand, active systems require an energy source for the actuators that apply external forces to the structure, which can supply or dissipate energy within the building as required. Similarly, semi-active systems are controllable passive devices with lower energy requirements than active systems, and they do not provide mechanical energy to the structural system. Hybrid or mixed systems are combinations of the previous types [7, 8].

One of the most used passive control techniques is foundation isolation systems, which reduce the effects of earthquakes on structures by isolating them from the ground

✉ A. Artunduaga
eivar.artunduaga@correounivalle.edu.co

S. Vides
sharick.vides@correounivalle.edu.co

B. Castillo
bryan.castillo@correounivalle.edu.co

J. Marulanda
johannio.marulanda@correounivalle.edu.co

P. Thomson
peter.thomson@correounivalle.edu.co

[1] School of Civil Engineering and Geomatic, Engineering Faculty, Universidad del Valle, Cali, Colombia

through devices such as friction pendulum bearings or elastomeric isolators, the latter being the most used. This separation of the structure from the ground is achieved by introducing a layer of low horizontal stiffness between the structure and its foundation [9], resulting in a higher period for the superstructure. This movement shifts it away from the dominant periods of the ground, leading to a reduction in acceleration and seismic energy [10]. The traditional approach to this control system focuses on energy dissipation through lateral deformations in the isolation layer, which are directly dependent on the type of isolators and the ratio between the vertical and horizontal stiffness of the devices. These displacements are considered in building codes, which prescribe separation distances between the insulated structure and neighbouring buildings. However, actual construction and operation are subject to human error and the characteristics of the potential seismic excitation. An example of a critical situation is resonance in the isolators, as it can cause excessive displacements that are usually not considered in the design process. In addition, in the case of seismic retrofitting of existing structures, this problem limits the use of this control system for those structures that do not have sufficient space to allow the necessary lateral displacement.

Although seismic isolation systems have been shown to reduce the seismic energy transmitted to the structure, thereby reducing vibrations in the upper floors, several studies have shown that in some cases they may not provide complete protection against damage to the building when large and unexpected displacements occur, [11]. This problem can lead to degradation or even destruction of the isolation system [12] and increases the likelihood of a building colliding with adjacent structures (13). This limitation has led to the exploration of hybrid control systems that combine base isolators with active or semi-active devices to enhance energy dissipation and adaptability in response to seismic excitations [14]. Within these hybrid systems, energy dissipation devices such as fluid viscous dampers and magnetorheological devices have been extensively studied for their ability to enhance seismic performance [15, 16]. These components offer dynamic control of structural stiffness and damping, improving the building's overall seismic resilience. In the works presented by [17] in 2014 and [18] in 2017, control systems consisting of elastomeric isolators and magnetorheological dampers were studied by numerical modelling and experimental tests, respectively. In both cases, the effectiveness of these devices, especially when integrated into hybrid systems, has been confirmed through numerical modelling and experimental tests, highlighting their potential in reducing base displacements and improving structural response compared to traditional base isolation methods [19].

Therefore, these systems must use optimal control parameters to achieve more reliable vibration reduction, so that the properties of the base isolation can adapt to possible changes in operational structural loads or seismic requirements. However, the experimental evaluation of medium or large civil structures poses a problem of space and cost, especially in laboratories that do not have the necessary equipment for such tests. To effectively evaluate the performance of these complex structural control systems, advanced simulation methods like Real-Time Hybrid Simulations (RTHS) have emerged. RTHS combines numerical and experimental substructures to provide a comprehensive assessment of the control systems' behaviour under dynamic conditions [4, 6, 20]. This technique involves dividing the structural system into an experimental substructure (ES), analysed using hydraulic actuators, and a numerical substructure (NS), which is simulated computationally [21–23]. RTHS offers significant advantages, including cost reduction, space efficiency, and enhanced structural evaluation compared to traditional shake table tests [19, 24]. This innovative technology has been used to evaluate magnetorheological and tuned liquid dampers [19, 24], as well as components of a single structure with multiple degrees of freedom [21]. The use of RTHS for the experimental analysis of hybrid control systems would provide research with the necessary flexibility to deal with variable structural parameters.

This methodology was used by [18] in 2010 to analyse a three-story structure with a magnetorheological (MR) damper on the first floor. Experimental evaluations were performed to evaluate semi-active control strategies, including clipped-optimal (bang-bang) control, clipped-optimal (force-tracking) control, overdriven back driven clipped-optimal (bang-bang) control, and overdriven back driven clipped-optimal (force-tracking) control. The results showed that the force-tracking controllers achieved excellent performance while maintaining relatively low damping forces in the device. In 2012, [25] proposed a type of hydraulic servo-tracking control based on models that include feedback loops to directly address additional undesirable dynamics in the RTHS loop. The results showed near-perfect tracking of the desired displacement signal. In addition, the study presented by [10] validated the performance of four semi-active control algorithms for a moment-resisting frame using a 200 kN MR damper on a large scale. Four semi-active controllers, named "passive-on", "clipped-optimal controller", "decentralized output feedback polynomial controller" and "Lyapunov stability-based controller", were designed and RTHS tests were performed under three different seismic excitations, revealing the differences found with each of the analysed approaches. In recent years, significant progress has been made in the implementation of RTHS, as shown by [18], where an evaluation of a structure with an intermediate seismic isolation system and semi-active damping was carried out. Furthermore, [20] proposed a force control method for the experimental evaluation of a concrete column that is part of the structural system of a bridge subjected to horizontal and vertical seismic movements. In 2020, [26] introduced a benchmark problem for tracking control during an RTHS of a structure subjected to dynamic forces. In [27], a Kalman filter-based compensation method was proposed to solve the benchmark problem. Several RTHS experiments were carried out to evaluate the performance of the proposed strategy, showing its effective improvement in accuracy, stability, and robustness in simulations. In the same year, [27] used RTHS to analyse the effect of adding viscous dampers to mitigate wind-induced vibrations in a 40-storey structure. Two large-scale viscous dampers were evaluated experimentally, while the rest of the system was modelled computationally, allowing the reduction in ground acceleration to be quantified. In 2021, [28] used RTHS to study a three-story steel space frame with Y-shaped eccentric braces, while in 2022, the methodology was used by [25] to characterize friction pendulum isolators with different surface treatments and by [29] to evaluate the efficiency of magnetorheological dampers in mitigating train-induced vibrations in bridges. This research focuses on the detailed evaluation of the seismic performance of low-rise buildings using structural control systems through RTHS. The systems evaluated include a hybrid control system incorporating base isolators and semi-active fluid viscous dampers. The quantitative and experimental approach aims to provide a deeper understanding and enhance the resilient design capacity of civil structures.

Methodology

Reference structure

A concrete frame building was selected as the reference structure for this study. The structure consists of 6 floors and 7 slabs, including the base insulation system, with a height of 17 m and an approximate floor area of 3037.5 m^2, as shown in Fig. 1. A total of 7 and 10 column lines were introduced in the X and Y directions respectively, resulting in 70 columns, each equipped with an isolator, as shown on the first floor Fig. 2a. Floors 2, 3, and 4 are shown in Fig. 2b and cover an area of 3037.5 m^2, while floors 5, 6, and 7 correspond to Fig. 2c with an area of 2362.5 m^2. The floor-to-floor height is 3 m for the first level and 2.8 m for the upper levels. The floor system consists of 20×45 cm beams supporting a 5.5 cm thick concrete slab, spaced at $75cm$ intervals along the Y-axis. A rigid membrane was assumed at all levels.

Modal analysis of the isolated structure was carried out, evaluating 24 modes, of which the first two represent more than 95% of the mass participation in the X and Y longitudinal axes. These modes have very close periods of 2.11 s for

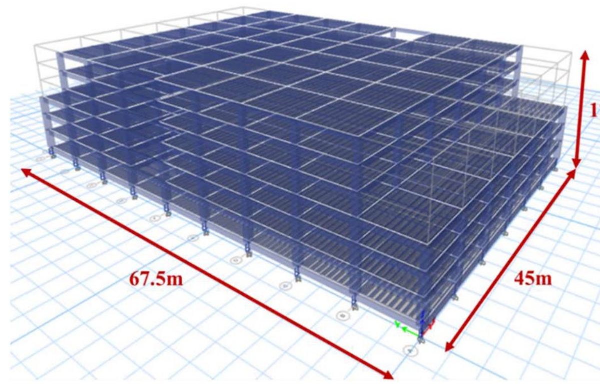

Fig. 1 3D model of reference structure

Mode 1 and 2.10 s for Mode 2, respectively, and demonstrate behavior like the motion of a rigid body in the X and Y directions, respectively. This is attributed to the use of a single type of isolator with identical properties in these directions. As for the base isolation system, elastomeric isolators reinforced with steel plates were chosen as they are the most used devices [4]. Preliminary sizing was performed following the procedure described in FEMA 450 and the method proposed by [30]. The isolators were modeled using ETABS19 software, considering a non-linear behavior for the longitudinal degrees of freedom in the X and Y directions, governed by the bilinear hysteresis model [21]. This model is defined by three primary stiffness parameters: effective stiffness K_{eff}, elastic stiffness K_1, and post-yield stiffness K_2, as defined in Eqs. (1) and (2). In addition, the dissipated energy E_D is presented as the area enclosed by a hysteresis loop and directly influences the force at zero displacement Q and the yield force F_y, calculated by Eqs. (3)–(5). For the axial degree of freedom, a linear behavior of the isolator was assumed, with the vertical stiffness K_v calculated using Eq. (6), taking the value of the effective damping β as 14%.

$$K_1 = \frac{Q + K_2 D_y}{D_y} \tag{1}$$

$$K_2 = K_{eff} - \frac{Q}{D_M} \tag{2}$$

$$E_D = 2\pi K_{eff} D_D^2 \beta_{eff} \tag{3}$$

$$Q = \frac{E_D}{4\left(D_M - D_y\right)} \tag{4}$$

$$F_y = Q + K_2 D_y \tag{5}$$

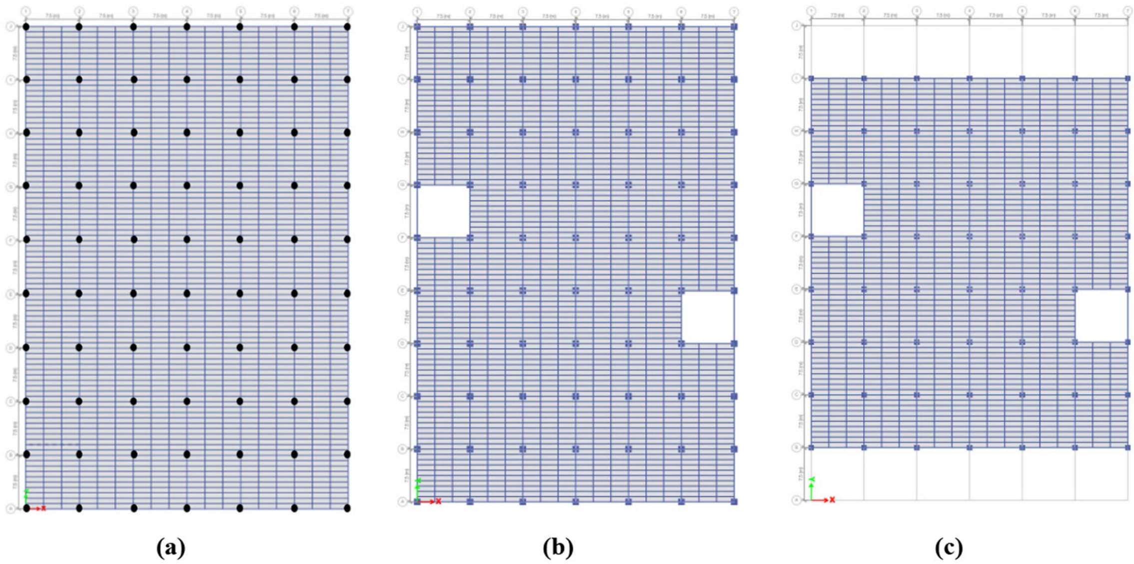

Fig. 2 **a** Floor 1 (base slab), **b** Floors 2, 3 and 4, **c** Floors 5, 6 and 7

$$K_v = \frac{E_{cf} \cdot A_{eff}}{Hr} \tag{6}$$

Variable orifice viscous fluid damper (VOD)

Viscous orifice dampers (VODs) are one of the most common semi-active hydraulic devices and typically consist of a variable force damper (VFD) with a mechanism that controls the viscous fluid flow, thus altering the reaction force of the device. Numerous studies, including those by [15, 21, 26], among others, have investigated the behavior of semi-active viscous fluid dampers, demonstrating their effectiveness in mitigating vibration in dynamically loaded structures. The behavior of VODs is controlled within a force range that varies as a function of the amount of flow passing through the orifice, providing a minimum value when the valve is fully open and maximizing when it is almost fully closed [15].

A small-scale viscous fluid damper was designed, consisting of an external cylinder of 210 mm stroke and 25.4 mm inner diameter, and a rod of 12.7 mm diameter on each side of the piston, to equalize the pressures in the two chambers without the need for an accumulator, with a total length of approximately 700 mm. To vary the force produced by the device, a DV08VN $^1/_4{}'$ needle valve was adapted to control the oil flow, changing the behavior of the force depending on the opening level, with a range from 0 to 7.3 turns; in position 0 (V0) the valve is fully open and the force is minimum, while in position 7.25 (V7.25) it approaches full closure and the force is maximum. A continuously rotating servomotor with dimensions of $5.4 \times 4.4 \times 2.0$ cm, an operating voltage of 4.8–6 V, and a minimum torque of 5.5 kg $*$ cm was installed in the valve and controlled by an ARDUINO DUE microprocessor.

In addition, to protect the piston rod and shock absorber seals, a relief valve system was designed with a maximum pressure of 2200psi, connected with flexible piping to each cylinder chamber to avoid excessive pressures in the event of total closure of the valve, which could cause damage to any of its components. To control the position of the needle valve, a coupling piece was installed between the servomotor and the valve head, which connects both components using teeth that engage circumferentially without leaving any space between them. The coupling piece has 32 holes that determine the position of the motor and calculate the speed at which it rotates. This measurement is made by the FC-03 sensor, whose infrared light detects the holes in the part and the time it takes to pass from one to the other.

In the experimental setup, the damper was placed on a metal frame made up of four $150 \times 50 \times 5$ mm rectangular section metal columns embedded in the base, interconnected with $100 \times 50 \times 10$ mm angles. To induce displacement of the device, one end of the rod was connected to the seismic table of the School of Civil Engineering and Geomatics (EICG) of the Universidad del Valle, through a rigid piece; between the table-damper connection, a load cell with a maximum capacity of 1.5 tones was installed to quantify the reaction force of the VOD, as shown in Fig. 3.

For the mechanical characterization of the VOD, seven sinusoidal displacement protocols were analysed, with an amplitude of $\pm$ 1 cm and frequencies ranging from 0.35 to 3 Hz. A key feature of VODs is the nonlinear behaviour observed in their force–displacement and force–velocity hysteresis cycles. Figure 4 illustrates the hysteretic response of

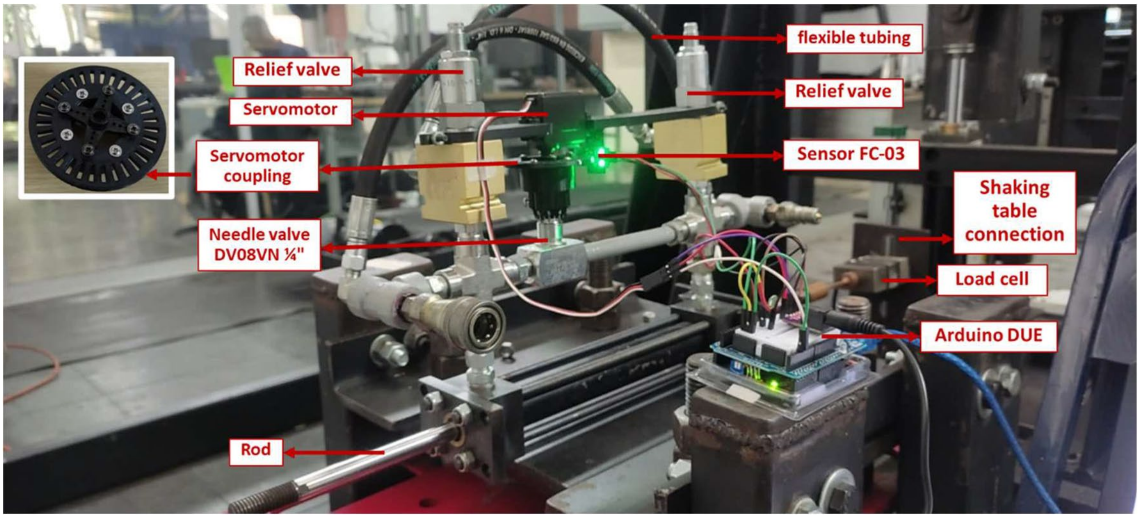

Fig. 3 Experimental damper assembly

the device tested under three different cases (100%, 31.51% and 4.11% of opening), each subjected to varying excitation frequencies. The increase in force as oil flow becomes restricted is clearly noticeable. Additionally, the excitation frequency significantly affects the damper's dynamic behaviour, as evidenced by the changing shape of the hysteresis loops with increasing frequency. An example is the 0.50 Hz frequency, where the hysteresis cycle highlights the strong influence of gasket friction on the device's reaction force. This behaviour is attributed to the cylinder's size, as friction forces in commercial devices are usually negligible compared to the viscous component due to the larger piston sizes.

Semiactive control strategy

Design of the optimal control law

Based on the linear quadratic control (LQR) theory which performs a systematic procedure [35], where the gain matrix K_{LQR} was determined. This matrix is associated with the control signal $F_{T-OPT}(t)$, as shown in Eq. (7), to minimize Eq. (8). Here, Q and R are positive definite matrices specifying the relative importance of the error and energy expenditure of the control signal.

$$F_{T-OPT}(t) = -\boldsymbol{K_{LQR}}x(t) \tag{7}$$

$$J = \int_0^\infty \left(x^T\boldsymbol{Q}x + u^T\boldsymbol{R}u\right)dt \tag{8}$$

If the performance indices are formulated in terms of system outputs Eq. (9), the optimal matrix can be calculated considering the importance of the system outputs, using Eq. (10) for the state vector-based adjustment Eq. (11).

$$J = \int_0^\infty \left(y^T\boldsymbol{Q}y + u^T\boldsymbol{R}u\right)dt \tag{9}$$

$$y = \boldsymbol{C}x \tag{10}$$

$$J = \int_0^\infty \left(x^T\boldsymbol{C_D^T}\boldsymbol{Q}\boldsymbol{C}x + u^T\boldsymbol{R}u\right)dt$$

where,

$$\boldsymbol{C_D} = \begin{bmatrix} 1 & 0 & 0 & 0 & 0 & 0 & 0 & 0 & 0 & 0 & 0 & 0 & 0 & 0 \\ -1 & 1 & 0 & 0 & 0 & 0 & 0 & 0 & 0 & 0 & 0 & 0 & 0 & 0 \\ 0 & -1 & 1 & 0 & 0 & 0 & 0 & 0 & 0 & 0 & 0 & 0 & 0 & 0 \\ 0 & 0 & -1 & 1 & 0 & 0 & 0 & 0 & 0 & 0 & 0 & 0 & 0 & 0 \\ 0 & 0 & 0 & -1 & 1 & 0 & 0 & 0 & 0 & 0 & 0 & 0 & 0 & 0 \\ 0 & 0 & 0 & 0 & -1 & 1 & 0 & 0 & 0 & 0 & 0 & 0 & 0 & 0 \\ 0 & 0 & 0 & 0 & 0 & -1 & 1 & 0 & 0 & 0 & 0 & 0 & 0 & 0 \end{bmatrix}$$

$$\boldsymbol{Q} = \begin{bmatrix} 0.01 & 0 & 0 & 0 & 0 & 0 & 0 \\ 0 & 1 & 0 & 0 & 0 & 0 & 0 \\ 0 & 0 & 1 & 0 & 0 & 0 & 0 \\ 0 & 0 & 0 & 1 & 0 & 0 & 0 \\ 0 & 0 & 0 & 0 & 1 & 0 & 0 \\ 0 & 0 & 0 & 0 & 0 & 1 & 0 \\ 0 & 0 & 0 & 0 & 0 & 0 & 1 \end{bmatrix} \quad \boldsymbol{R} = [10e - 12] \tag{11}$$

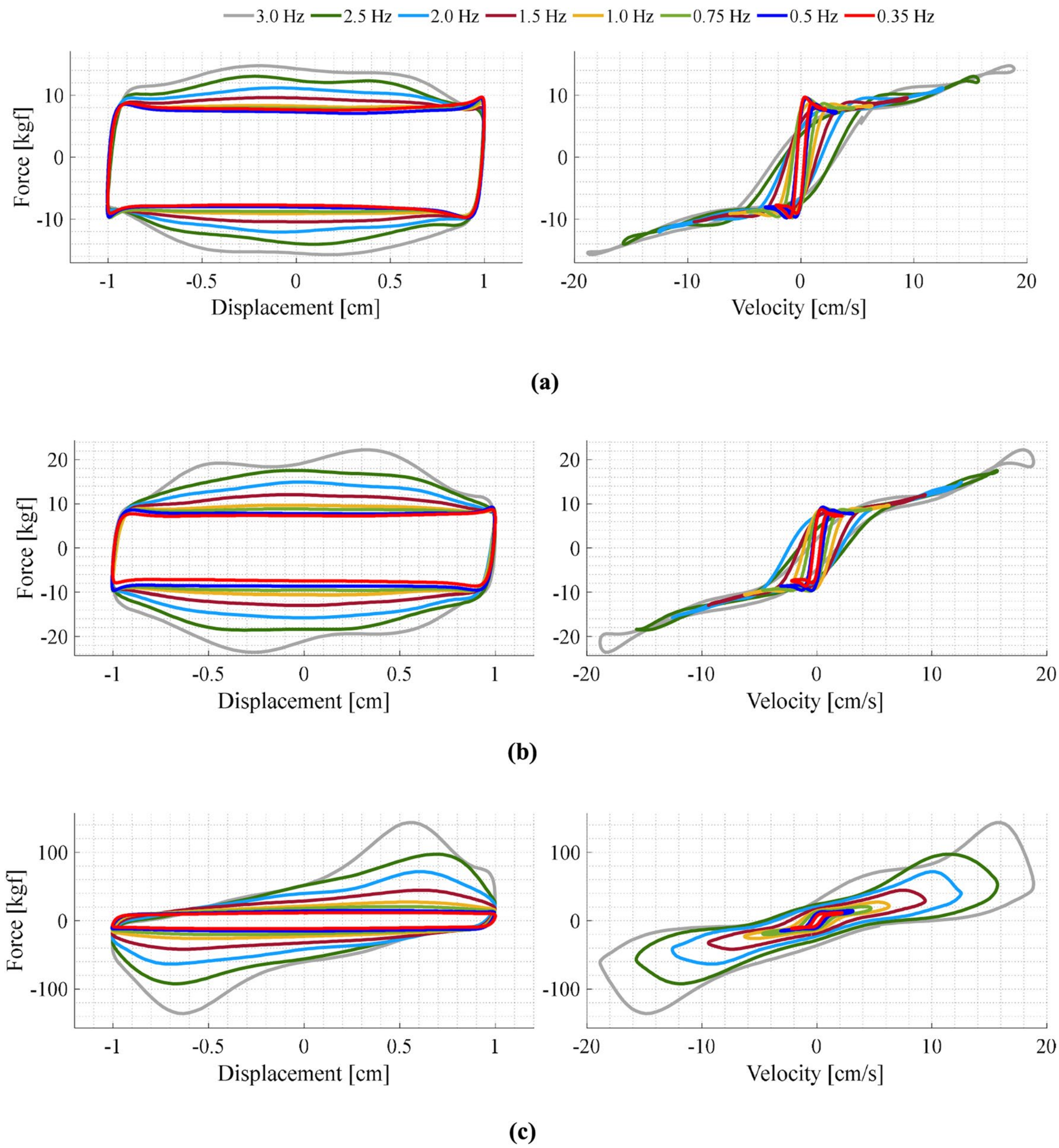

Fig. 4 Calibration VOD—Hysteresis cycles. **a** 100% of opening, **b** 31.51% of opening, **c** 4.11% of opening

In this study, the objective is to minimize the base displacements (x_1) and ground drifts using the control signal F_{T-OPT}.

However, this involves measuring each of the states with a sensor or a combination of sensors, the cost and complexity of which pose problems in experimental testing. Typically, only a portion of the states is easily measurable and thus available for system feedback [36]. To address this limitation, a Kalman filter was employed as a state estimator and integrated into the controller (Fig. 4). In this scenario, the structure is subjected to a seismic excitation $\ddot{u}_g$, and the response y_t in the degrees of freedom (DoF) of interest is calculated. In addition, the instrumented DoFs measure the actual response (y_m), which represents the measured state and is used to feed the estimator. The Kalman filter, in turn, establishes an inner loop by requiring feedback from the control signal $\left(F_{T-OPT}\right)$ to estimate the other states and close the outer loop of the system. This methodology is known as linear quadratic Gaussian (LQG) control. The design of this approach considered the force limits of the device and the response time of the motor. In addition, covariance matrix values for the noise w and v were used as $Q_w = 1e3$ and $R_v = 1e-1$, respectively.

Clipped optimal control strategy for VOD force variation

The Trimmed Optimal Control strategy was used to manage the VOD force variations [11]. The controller was designed as a function of the force and direction of rotation of the servo motor. This process was developed in Simulink using a low-cost microprocessor, the Arduino Due, with a sampling rate of 150 Hz. According to the dynamic characterization of the VOD, the force increases as the valve closes and decreases as it opens. Therefore, the control motor signal was set as a function of the direction of rotation of the servomotor, with 90° as the command to open the valve at maximum speed, – 90° to close it, and 0° to stop its movement. In this context, the control algorithm is based on the force error as described in Eq. (12), where F_{OPT} represents the optimum desired force for a damper, and F_{VOD} is the measured force of the device. The motor control signal u_{motor} is calculated according to Eq. (13), where F_{tol} represents the force tolerance of the VOD, considering the noise in the load cell measurement, and F_{max} presents the maximum force the device can withstand. In summary, it is important to note that the last two mentioned rules have been implemented to protect the VOD and avoid damage to its rod. The complexity of the VOD behavior owing to the variability of the force as a function of the flow opening, highlights the need for future research to implement a more robust (PID, H_∞ or μ) controller that can accurately replicate the reference signal increasing the simulation performance.

$$e_F = |F_{OPT}| - |F_{VOD}| \tag{12}$$

$$u_{motor}(e_F, F_{VOD}) = \begin{cases} 90 & if \quad e_F < -F_{tol} \rightarrow Open \\ 0 & if \quad -F_{tol} \le e_F \le F_{tol} \rightarrow Stop \\ -90 & if \quad e_F > F_{tol} \rightarrow Close \\ 90 & if \quad F_{VOD} \le -F_{max} \rightarrow Open \\ 90 & if \quad F_{VOD} \ge F_{max} \rightarrow Open \end{cases} \tag{13}$$

Figure 4 shows a block diagram of the operation of the VOD force control system. Initially, this system is fed with the measured displacement u_{1_m}, which is scaled and converted into the measured state x_{1_m}, which serves as the first input to the Kalman filter. The Kalman filter, in turn, takes care of estimating all states $\hat{x}$ and calculates the desired total force F_{T-OPT} noting that this value represents the required action of the dampers in the complete system. This force is then adjusted by the scaling factor E_f and divided by the number of added devices N_{VOD} to determine the optimum force required for each device, F_{OPT}. The force error e_F feeds the control law that calculates the motor signal u_{motor}. Finally, the measured force F_{VOD} is multiplied by the corresponding scale to feedback to the Kalman filter and closes the outer loop of the system (Fig. 5).

Real-time hybrid simulation

Numerical substructure (NS)

To define the structural natural frequency (NS), a numerical simplification of the representative structure described above was performed, assuming a rigid diaphragm condition for each floor of the building with a single degree of freedom (1 DoF) system per floor. Since Eq. (14) governs the behavior of the

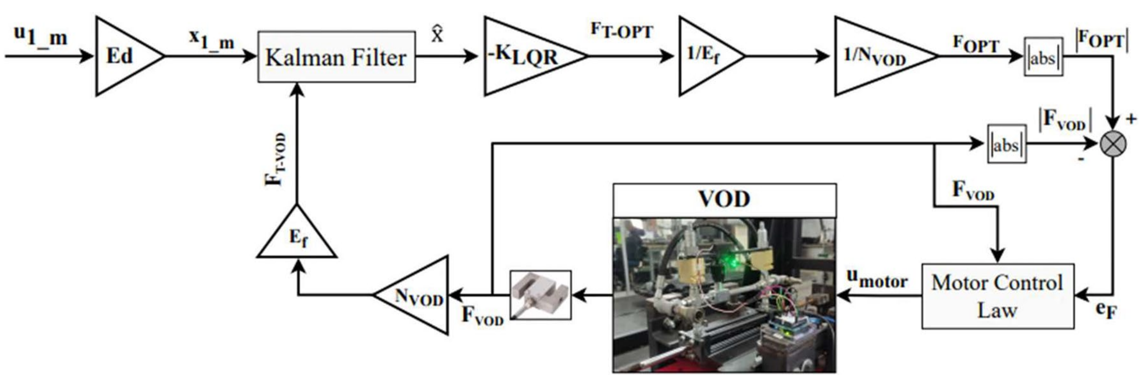

Fig. 5 Block diagram of the VOD control

structure, a model was fitted whose matrices $\boldsymbol{M}$, $\boldsymbol{C}$, and $\boldsymbol{K}$ are given by the following form:

$$\boldsymbol{M}\ddot{u} + \boldsymbol{C}\dot{u} + \boldsymbol{K}u = -\boldsymbol{M}\Gamma\ddot{u}_g \tag{14}$$

where,

$$\boldsymbol{M} = \begin{bmatrix} m1 & & & & & & \\ & m2 & & & & & \\ & & m3 & & & & \\ & & & m4 & & & \\ & & & & m5 & & \\ & & & & & m6 & \\ & & & & & & m7 \end{bmatrix}$$

$$\boldsymbol{C} = \begin{bmatrix} c1+c2 & -c2 & & & & & \\ -c2 & c2+c3 & -c3 & & & & \\ & -c3 & c3+c4 & -c4 & & & \\ & & -c4 & c4+c5 & -c5 & & \\ & & & -c5 & c5+c6 & -c6 & \\ & & & & -c6 & c6+c7 & -c7 \\ & & & & & -c7 & c7 \end{bmatrix} \tag{15}$$

$$\boldsymbol{K} = \begin{bmatrix} k1+k2 & -k2 & & & & & \\ -k2 & k2+k3 & -k3 & & & & \\ & -k3 & k3+k4 & -k4 & & & \\ & & -k4 & k4+k5 & -k5 & & \\ & & & -k5 & k5+k6 & -k6 & \\ & & & & -k6 & k6+k7 & -k7 \\ & & & & & -k7 & k7 \end{bmatrix} \tag{16}$$

The state-space model described in Eqs. (15) and (16) was formulated, with matrices **M**, **C**, and **K** containing the parameters adjusted using the dynamic response of the structure obtained from ETABS. Additionally, semi-active viscous fluid dampers (VOD) were introduced at the isolated base, as depicted in Fig. 6, to mitigate the displacements of that degree of freedom while minimizing any disruptions to the behavior of upper-level drifts. Where $\ddot{u}$, $\dot{u}$ and u are vectors of acceleration, velocity, and relative displacement, respectively, F_{VOD} is the control force produced by the dampers, $\Psi = [1000000]^T$ and $\Gamma = [1111111]^T$ The influence vectors for the VOD force and the inertial forces, and $\ddot{u}_g$ is the ground acceleration.

$$\begin{Bmatrix} \dot{u} \\ \ddot{u} \end{Bmatrix} = \begin{bmatrix} 0 & I \\ -M^{-1}K & -M^{-1}C \end{bmatrix} \begin{Bmatrix} u \\ \dot{u} \end{Bmatrix} + \begin{bmatrix} 0 & 0 \\ -I\Gamma_g & -M^{-1}\Psi \end{bmatrix} \begin{Bmatrix} \ddot{u}_g \\ F_{VOD} \end{Bmatrix} \tag{17}$$

$$\begin{Bmatrix} u \\ \dot{u} \end{Bmatrix} = \begin{bmatrix} I & 0 \\ 0 & I \end{bmatrix} \begin{Bmatrix} u \\ \dot{u} \end{Bmatrix} + \begin{bmatrix} 0 & 0 \\ 0 & 0 \end{bmatrix} \begin{Bmatrix} \ddot{u}_g \\ F_{VOD} \end{Bmatrix} \tag{18}$$

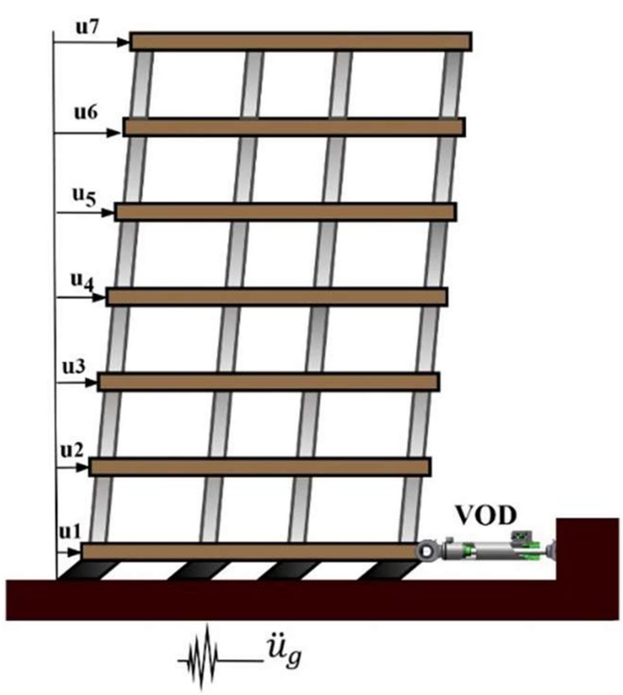

Fig. 6 Simplified scheme of the reference structure with the addition of VOD

Input signal: seismic excitation

Five earthquakes were chosen for real-time hybrid simulations (RTHS), corresponding to El Centro (USA 1940), Pizarro (Colombia 2004), Chihuahua (Mexico), Kobe (Japan 1995), and Loma Prieta (USA 1989); these signals were scaled with a maximum value of 2.45 m/s^2, corresponding to 0.25 g. Figure 6 shows the frequency content of the five selected events, focusing on values below 10 Hz.

RTHS scheme

In this study, the transfer system chosen was the shaking table of the Faculty of Civil Engineering and Geomatics of the Universidad del Valle, consisting of a 1.1m × 1.5m aluminum plate supported on low-friction linear rails, coupled to a 45kN hydraulic actuator controlled by two 15gpm servo valves. The devices included an internal linear variable differential transformer (LVDT) to accurately measure piston displacement, driven by a hydraulic pump.

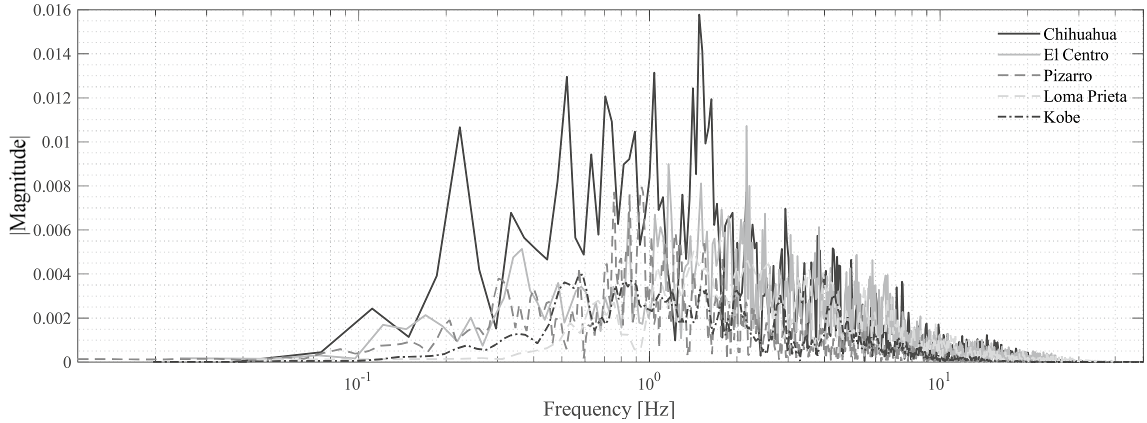

Fig. 7 Frequency content analysis of evaluated earthquakes

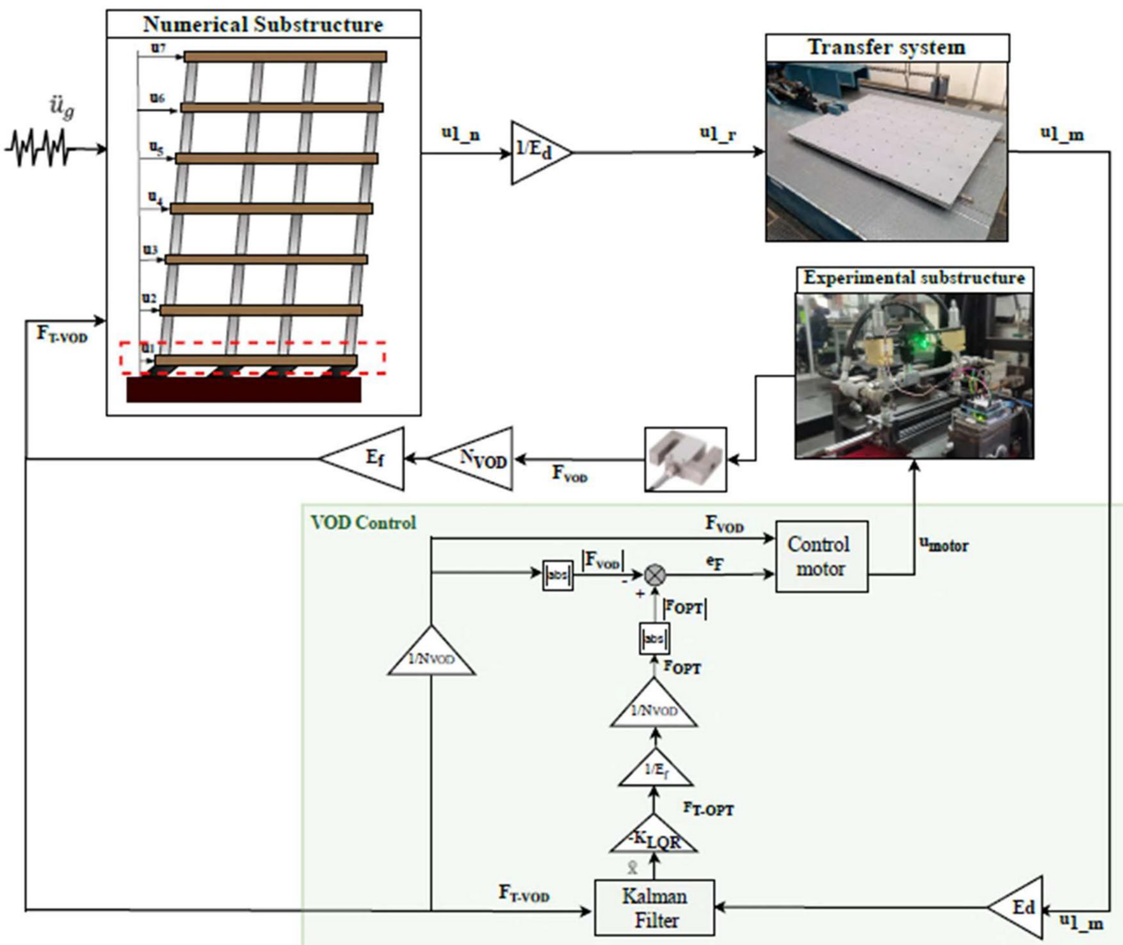

Fig. 8 RTHS Scheme with semi-active damper

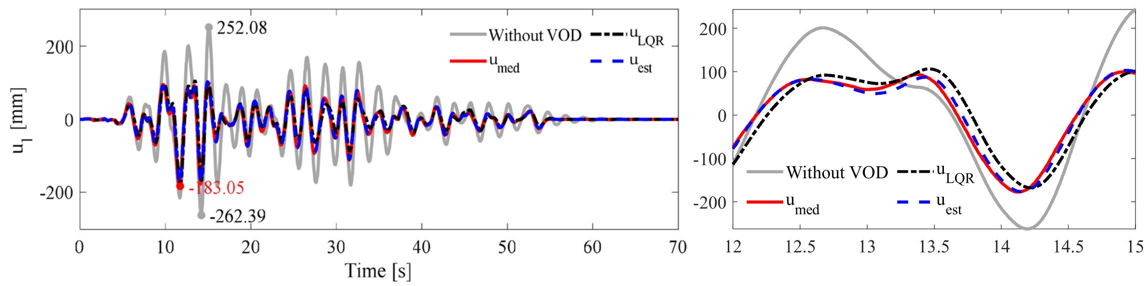

Fig. 9 Reduction of base displacements, Chihuahua earthquake

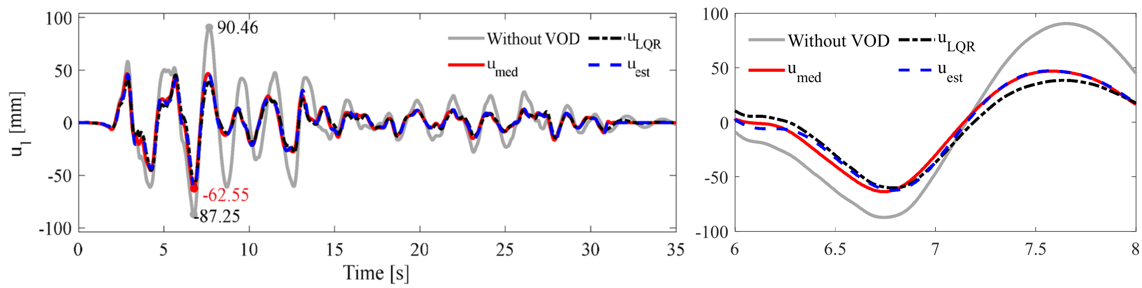

Fig. 10 Reduction of base displacements, El Centro earthquake

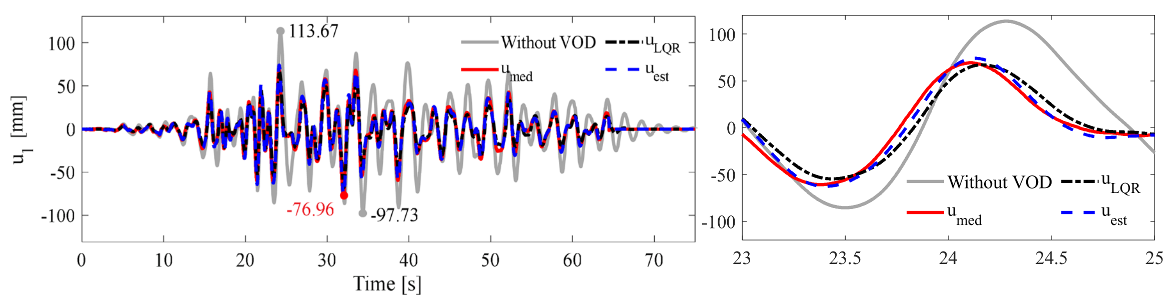

Fig. 11 Reduction of base displacements, Pizarro earthquake

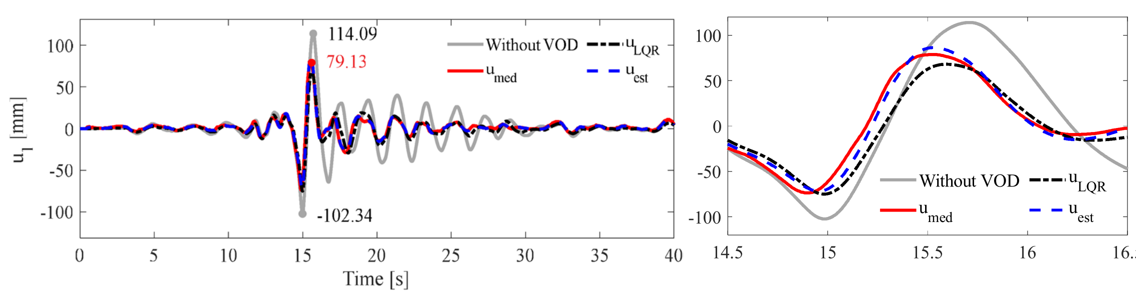

Fig. 12 Reduction of base displacements, Loma Prieta earthquake

For the RTHS, the scheme shown in Fig. 7 was used under the five seismic excitations described above. There it is demonstrated how the SN is subjected to the input signal $\ddot{u}_g$, and the response at degree of freedom 1 u_{1_n}, corresponding to the isolated base, is measured. These measurements were scaled using the E_d factor to determine the reference signal u_{1_r} effectively replicating the transfer system. The measured displacement u_{1_m} was processed through a Kalman filter to estimate the system states $\hat{x}$ and then forwarded to the optimal matrix K_{LQR} to calculate the total optimal force F_{T-OPT}. This value is divided by the number of devices N_{VOD} to establish the F_{OPT} force to be replicated by the damper. In real-time, the device controller compared F_{OPT} with the measured signal F_{VOD}, to obtain the force error e_F that feeds the motor controller and generates the u_{motor} command sent to VOD. The damper then responded, and the force was measured, scaled, and transmitted to the NS and Kalman filter, effectively closing the inner and outer loops of the system (Fig. 8).

Results

From Figs. 9, 10, 11, 12, the variations in base displacements are presented for the Chihuahua, El Centro, Pizarro, Loma Prieta, and Kobe earthquakes, respectively. The red line represents the displacement measured during the RHTS, while the grey line represents the behavior of the structure with conventional isolation systems, without the addition of VODs. In addition, the black line represents the optimal displacement values calculated using the LQR controller, and the blue line is the Kalman filter estimate. In all cases, it is evident that the filter accurately estimates the measured state and the LQG controller guarantees very similar displacement values to those obtained with LQR. Furthermore, a substantial reduction of the maximum base shifts is observed, amounting to 30.24%, 30.85%, 29.66%, 30.64%, and 44.39% for the five cases analyzed.

Figure 13 shows a frequency comparison between the optimal offset (u_{LQR}) and the offset obtained using the VOD controller (u_{med}) for all RTHS experiments. The upper left graph shows the fast Fourier transform of the measured signal, revealing that these shifts occur predominantly within a frequency range below 1.0 Hz, thus focusing the analysis on this range. The upper right graph shows the magnitude of the transfer function between u_{LQR} and u_{med} with mean values of 1.04, 1.02, 1.16, 1.06, and 1.12, and maximum values of 2.20, 1.50, 1.54, 1.77 and 4.28 for the five earthquakes analyzed, respectively. The lower graphs show the phase angle and the delay between the signals, the latter being less than 5 ms in all cases. From this it can be concluded that there was a good approximation to the optimal displacement, considering the non-linearity of the VOD and the response time of the engine.

In Table 1, the difference in energy dissipation between the structure with structural control devices and the conventional structure is clearly illustrated. The results indicate that the energy dissipation in the structure equipped with control devices is approximately 50% higher compared to the normal structure. This significant improvement highlights the effectiveness of control devices in optimizing structural behavior in response to external events.

Figure 14 shows the relative ground displacements obtained with the structure isolated from the base (grey line), with the optimal controller (black line), and during the RTHS (red line). As with the base displacement, a similar behavior to the optimum (LQR) was observed, with the expected variations due to the differences between the signals described above. Additionally, Table 2 summarizes the peak values for each floor, comparing the isolated structure

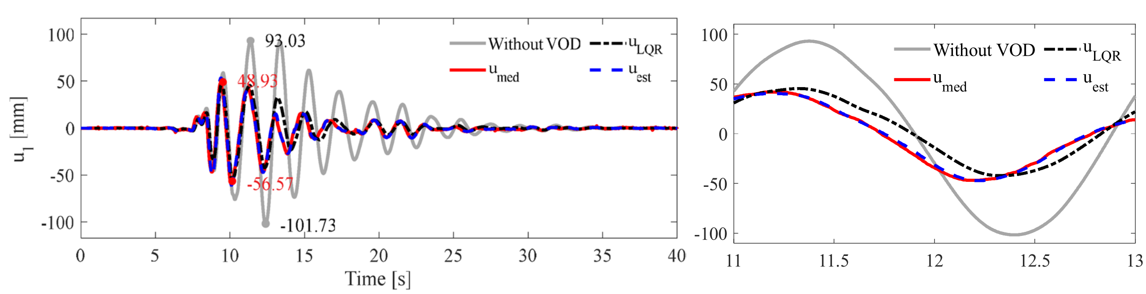

Fig. 13 Reduction of base displacements, Kobe earthquake

Table 1 Energy dissipation

Chihuahua		El Centro		Pizarro		Loma Prieta		Kobe	
ISO-VOD	VOD	ISO-VOD	VOD	ISO-VOD	VOD	ISO-VOD	VOD	ISO-VOD	VOD
1.000	1.443	1.000	1.230	1.000	1.419	1.000	1.490	1.000	1.603

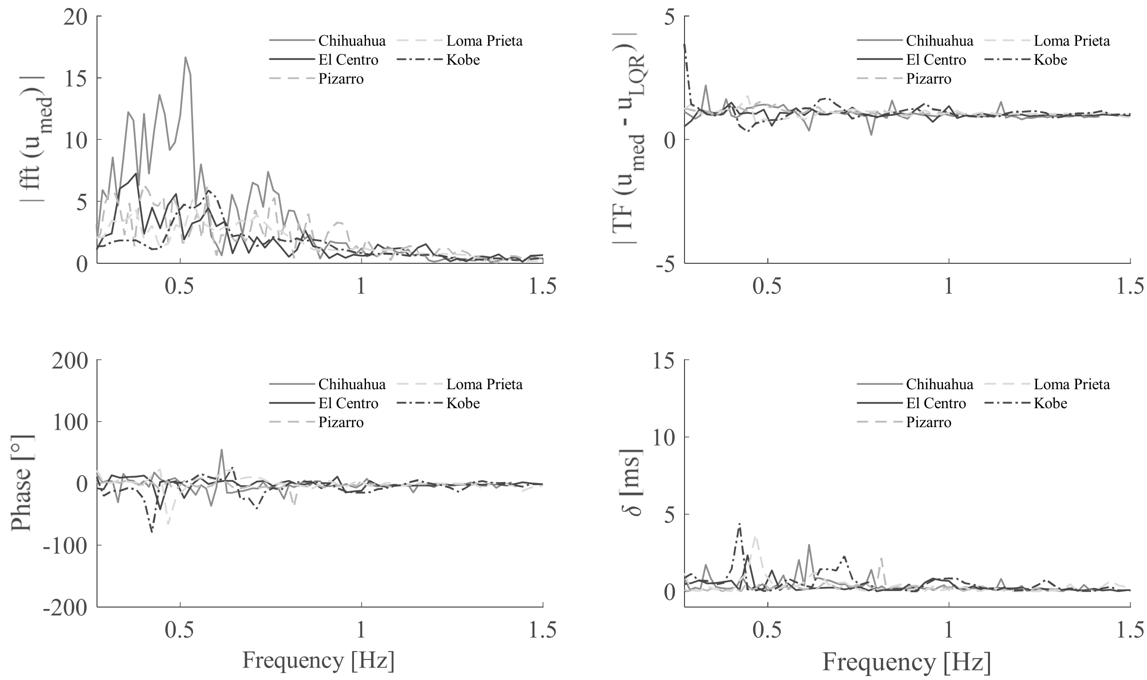

Fig. 14 Frequency response $u_{med} - u_{LQR}$

with the measured values. The optimum displacements are reduced at some points with respect to the isolated system and increased at others, with the percentage variation remaining below 36% in all cases. Furthermore, the relative displacements measured with the hybrid system (Isolators + VOD) faithfully reproduce those obtained with LQR, with small variations of less than 30%.

From Figs.15, 16, 17, 18, 19, the force behavior for the five earthquakes analyzed during the RTHS is shown. The black line represents the optimum force F_{OPT}, and the red line represents the force measured by the VOD load cell. As expected, the device is not able to perfectly reproduce the reference signal due to the limitations in the dynamic characterization and the delay present in the simulation. However, it is observed that the VOD can increase its force up to the maximum values and decrease it, when necessary, with variations of 2.58%, 15.37%, 36.08%, 10%, and 18.58% for the maximum force and 18.81%, 1.23%, 0.24%, 24.10% and 15.49% for the RMS between F_{OPT} and F_{VOD}.

Table 3 shows the energy dissipated by the VOD during the RTHS compared to the optimal case. Unlike the Kobe earthquake, in the other cases of analysis, the difference between the optimum and the obtained value does not exceed 20%, which shows a good performance of the device despite not obtaining perfect tracking of the force. These differences were to be expected due to the non-linearity of the VOD, the noise during measurement, and the low cost of the instrumentation and control system. However, during the tests, good performance of the hybrid control system was demonstrated by reducing the displacement at the base, while maintaining good behavior in ground drifts.

RTHS evaluation

During the application of the RTHS, discrepancies arise between the reference signal and the measured signal. These errors arise from factors inherent to the methodology, such as differences between the SN model and the real structure, electronic noise present in the SE experimental signals, and the dynamics of the actuators that are part of the transfer systems, among others [37]. For this reason, several indices have been proposed to evaluate the accuracy of RTS, taking these factors into account. Many of these evaluation measures focus on the local response during a hybrid simulation, considering the physical component and its interaction with the numerical component. The evaluation of the local performance is based on the synchronization of the boundary conditions between the numerical response (target displacement $u^*_{i,d}$) sent to the actuator and the actual displacement achieved (measured displacement $u^*_{i,m}$). The normalized root mean square in the experiment (NRMSE) can be used, according to [17], to obtain a single value representing this difference between the measured and target displacements in the time domain. For the frequency domain comparison, [18–22], corresponding to the frequency evaluation index (*FEI*), which compares the fast Fourier transform (FFT) of the desired signal $U^*_{i,d}$ with the measured signal $U^*_{i,m}$ at the actuator, the frequency with the most significant

Table 2 Reduction of relative floor displacements

u	Chihuahua			Centro			Pizarro			Loma Prieta			Kobe		
	Without VOD	RTHS	Red [%]	Without VOD	RTHS	Red [%]	Without VOD	RTHS	Red [%]	Without VOD	RTHS	Red [%]	Without VOD	RTHS	Red [%]
u_2	11.48	9.68	15.68	4.01	3.38	15.71	5.00	5.09	− 1.80	5.04	4.97	1.39	4.45	3.98	10.56
u_3	10.29	8.64	16.03	3.65	2.96	18.90	4.52	5.06	− 11.95	4.59	4.59	0.00	4.00	3.69	7.75
u_4	8.82	7.42	15.87	3.18	2.50	21.38	3.91	4.85	− 24.04	3.99	4.40	− 10.28	3.44	3.20	6.98
u_5	8.29	7.41	10.62	2.99	2.61	12.71	3.66	4.31	− 17.76	3.79	4.15	−9.50	3.18	3.31	−4.09
u_6	6.43	5.33	17.11	2.32	2.53	−9.05	2.86	3.61	−26.22	3.03	3.58	− 18.15	2.45	2.80	− 14.29
u_7	4.50	4.36	3.11	1.62	2.00	−23.46	2.03	2.75	−35.47	2.18	2.76	−26.61	1.70	2.22	−30.59

involvement during the RTHS f_{eq}, the generalized amplitude A_0 and the delay δ, respectively [37].

$$NRMS_{error} = \sqrt{\frac{\sum_{k-1}^{N}\left[u_{i,d}^{*}(k) - u_{i,m}^{*}(k)\right]^2}{\sum_{k-1}^{N}\left[u_{i,d}^{*}(k)\right]^2}} \tag{19}$$

$$FEI = \sum_{j-1}^{N}\left(\frac{U_{i,m}^{*}(j)}{U_{i,d}^{*}(j)} \cdot \frac{U_{i,d}^{*}(j)^l}{\sum_{j-1}^{P} U_{i,d}^{*}(j)^l}\right) \tag{20}$$

$$f^{eq} = \frac{\sum_{j-1}^{N}\left(U_{i,d}^{*}(j)^l \cdot f_i\right)}{\sum_{j-1}^{N} U_{i,d}^{*}(j)^l} \tag{21}$$

$$A_0 = FEI \tag{22}$$

$$\emptyset = arctan\left[\frac{Im(FEI)}{Re(FEI)}\right] \tag{23}$$

$$\delta = -\frac{\emptyset}{2 \cdot \pi \cdot f^{eq}} \tag{24}$$

On the other hand, the global indices consider the interaction between the numerical and experimental substructures, and in this research, they were evaluated in the time domain, quantifying the largest difference between the calculated and measured displacements, using e_{DM} and e_{MD}, as shown in [23] and [24].

$$e_{DM} = \frac{\left|\left|u_{i,d}^{*}\right|^{max} - \left|u_{i,m}^{*}\right|^{max}\right|}{\left|u_{i,m}^{*}\right|^{max}} \tag{25}$$

$$e_{MD} = \frac{\left|u_{i,d}^{*} - u_{i,m}^{*}\right|^{max}}{\left|u_{i,m}^{*}\right|^{max}} \tag{26}$$

Figures 20, 21, 22, 23, 24 shows the tracking of the transfer system for all RTHS performed. In addition, Table 3 presents the evaluation indicators where good tracking is shown, as the seismic table can reproduce the desired displacement in an optimal way, with generalized amplitude values very close to 1.0, NMRS errors lower than 5% and delays lower than 1 ms in all cases of analysis, so that the reliability of the RTHS can be affirmed (Fig. 25).

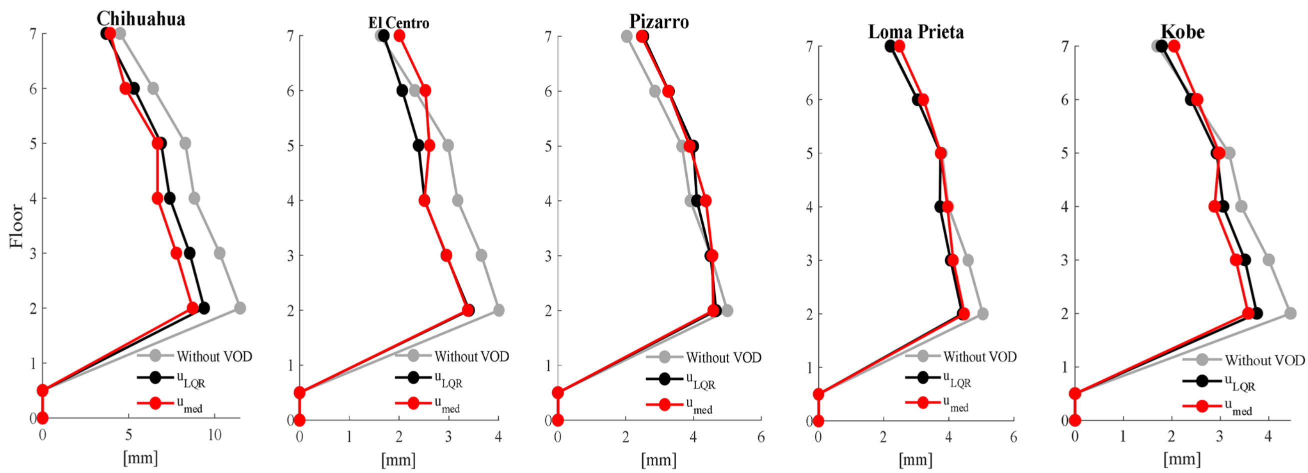

Fig. 15 Floor relative displacements

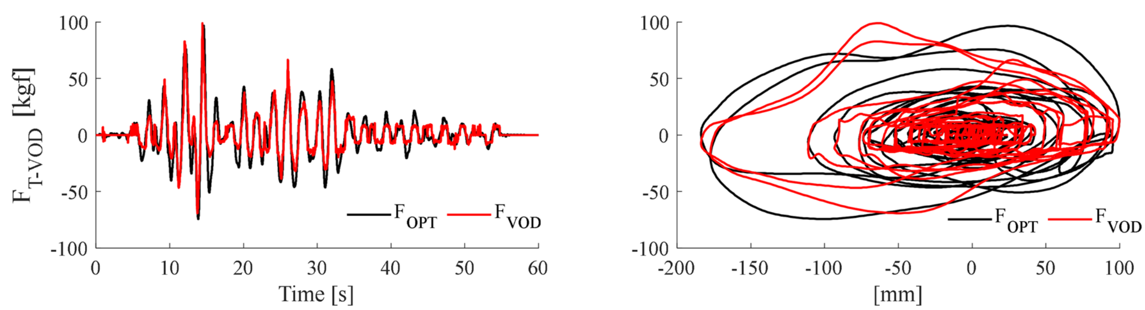

Fig. 16 VOD Force behavior during RTHS—Chihuahua

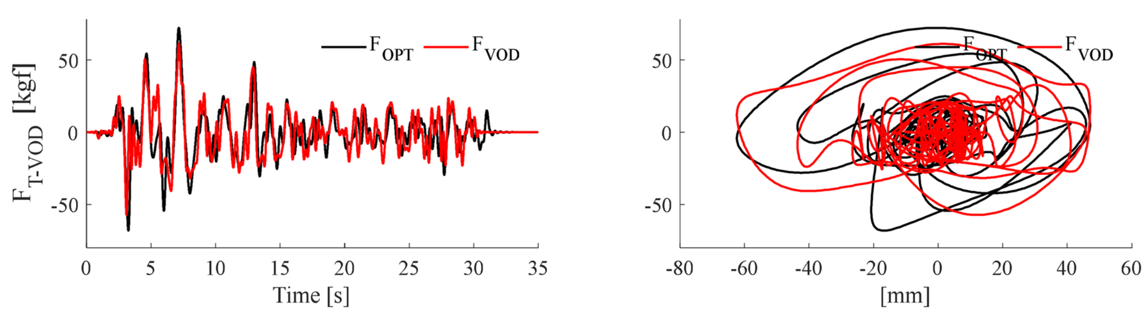

Fig. 17 VOD Force behavior during RTHS—El Centro

Conclusions

This research demonstrated the efficacy of using RTHS for evaluating the seismic performance of low-rise buildings equipped with hybrid control systems, including base isolators and semi-active viscous fluid dampers, such as substructure experiments in the simulation. The results showed that the use of semi-active control systems in conjunction with base isolators resulted in a significant reduction in base

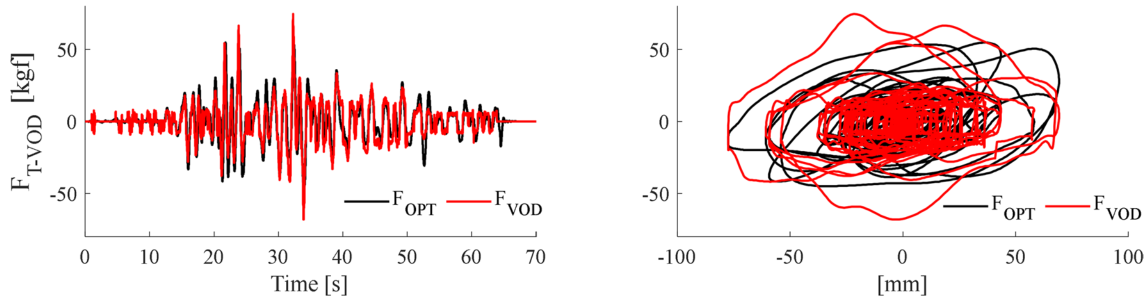

Fig. 18 VOD Force behavior during RTHS—Pizarro

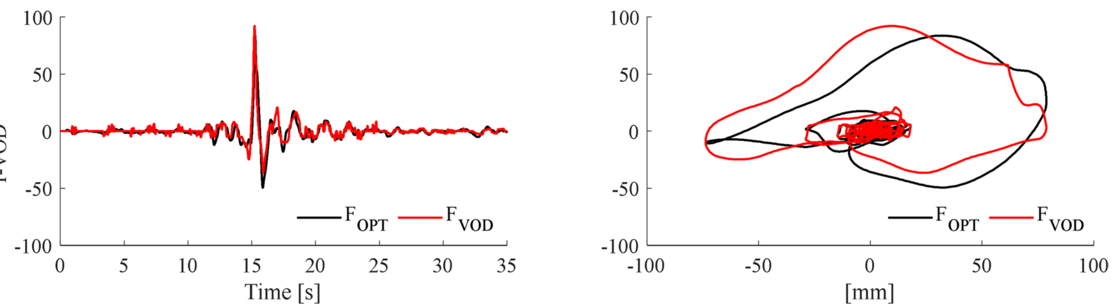

Fig. 19 VOD Force behavior during RTHS—Loma Prieta

Table 3 Hysteresis loop area

Case	$Area_{opt}$[kgf ∗ m]	$Area_{RTHS}$[kgf ∗ m]	*Diff* [%]
Chihuahua	141.48	113.41	19.84
El Centro	24.67	24.86	0.79
Pizarro	54.72	62.80	14.76
Loma Prieta	12.91	13.35	3.42
Kobe	18.99	13.65	28.13

displacements during seismic excitations, as evidenced by reductions of up to 44.39% across different earthquake scenarios. This highlights the capacity of hybrid systems to adaptively manage seismic energy dissipation, thus enhancing structural resilience.

The implementation of a Kalman filter-based Linear Quadratic Gaussian (LQG) controller demonstrated high

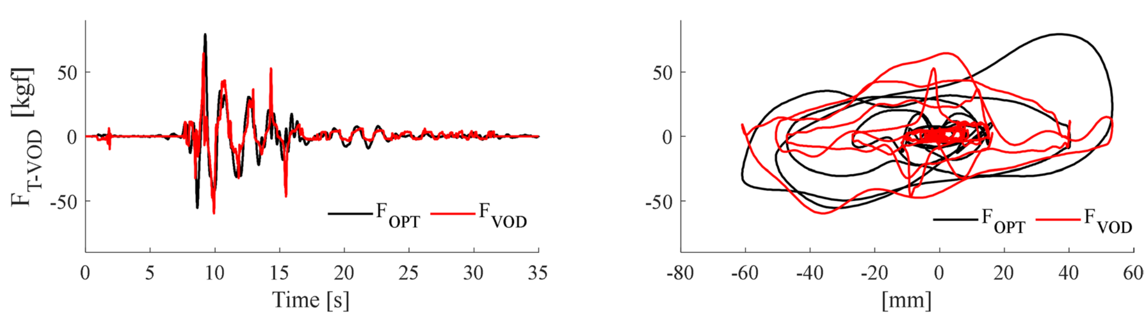

Fig. 20 VOD Force behavior during RTHS—Kobe

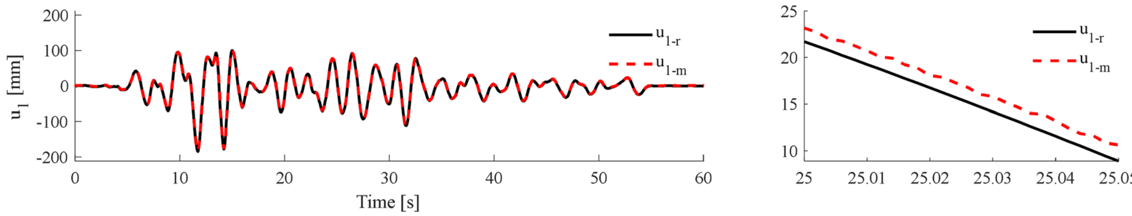

Fig. 21 Tracking transfer system—Chihuahua

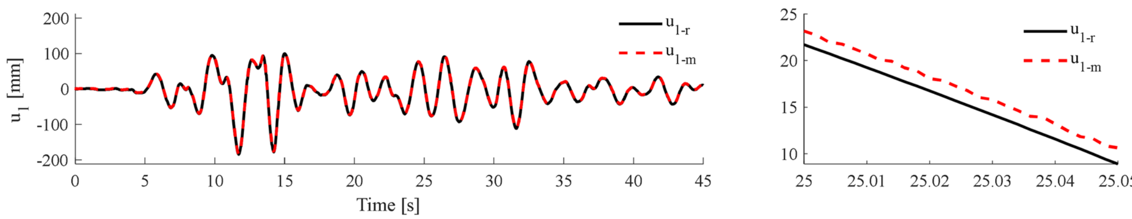

Fig. 22 Tracking of transfer system—El Centro

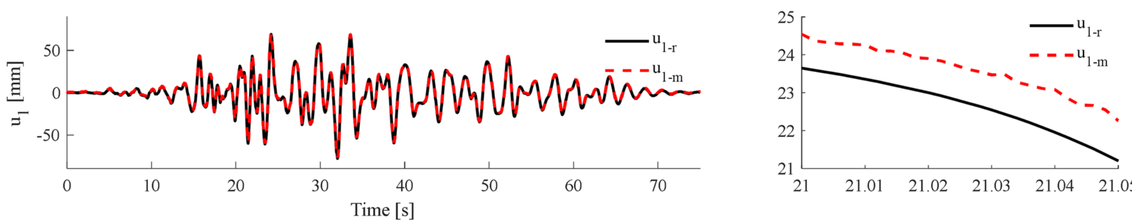

Fig. 23 Tracking of transfer system—Pizarro

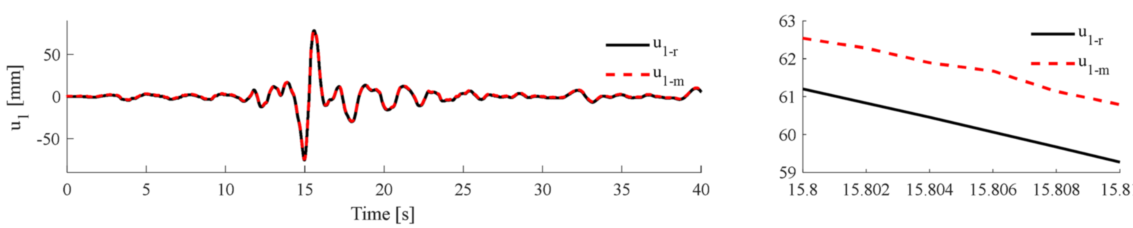

Fig. 24 Tracking of transfer system—Loma Prieta

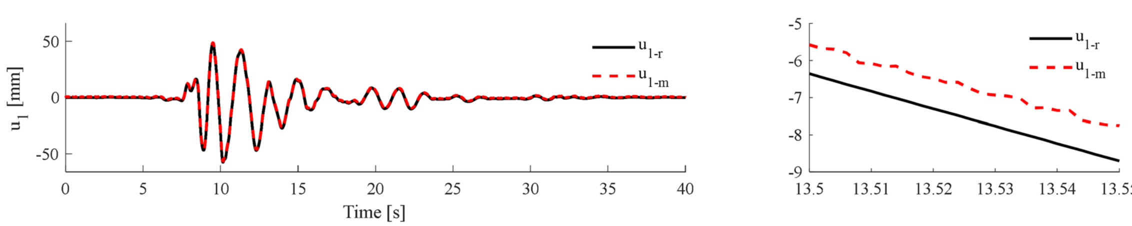

Fig. 25 Tracking of transfer system—Kobe

precision in tracking the desired structural responses with minimal delay and strong correspondence between the measured and reference signals. This study confirms that these control strategies can reliably manage the nonlinear behavior of viscous dampers, achieving near-optimal performance despite the inherent complexity of the system.

The RTHS methodology has been proven to be a cost-effective and efficient tool for assessing the dynamic performance of complex structural control systems. This approach allows for detailed experimental analysis without the need for full-scale testing, offering significant benefits in terms of cost, space efficiency, and adaptability to varying structural conditions.

Despite these promising outcomes, further research is required to refine the control algorithms for improved performance under various seismic conditions. The nonlinearity of the dampers and instrumentation limitations suggest that future studies should focus on more advanced control methods, such as PID or H∞ controllers, to enhance robustness and minimize discrepancies between experimental and optimal results.

Acknowledgements This research is part of the research project "Real-Time Hybrid Simulations: A Reliable, Fast, and Cost-Effective Alternative for the Evaluation of Resilient Structures," within the framework of the Emerging Technologies for Seismic Risk Mitigation in Civil Infrastructure program, CT 80740-463-2020. The authors would like to express their gratitude to the University of Valle and the Ministry of Science, Technology, and Innovation (Minciencias), which provided funding for this program.

Funding Open Access funding provided by Colombia Consortium. This work was funded by the Universidad del Valle and the Ministry of Science, Technology and Innovation (Minciencias), through the Emerging Technologies for Seismic Risk Mitigation in Civil Infrastructure program, with Grant number CT 80740-463-2020. Likewise, all authors certify that they have no affiliations or participation in any organization or entity with any financial or non-financial interest in the subject or materials discussed in this manuscript.

Declarations

Conflict of interest The authors declare that there is no conflict of interest regarding the publication of this article.

Ethical approval This study did not involve human participants or animals, and therefore ethical approval was not required.

References

1. Dyke SJ, Stojadinovic B, Arduino P, Garlock M, Luco N, Ramirez JA et al (2010) Community workshop: 2020 vision for earthquake engineering research in the USA. In: Proceedings of 15th world conference on earthquake engineering (15WCEE) (Figure 1)
2. Castillo B, Vides SM, Hoyos AF, Thomson P, Marulanda J (2022) Simulaciones Híbridas en Tiempo-Real SHTR aplicadas en la evaluación del desempeño dinámico de muros delgados de concreto reforzado afectados en una edificación aislada. Ingeniería y Desarrollo en la Nueva Era [Internet]. Available from: https://doi.org/10.5281/zenodo.7381846
3. Gómez D, Marulanda J, Thomson P (2008) Sistemas de control para la protección de estructuras civiles sometidas a cargas dinámicas control systems for dynamic loading protection of civil structures. Año 75
4. Castillo Torres B, ArtunduagaTriviño EA, Marulanda Casas J, Ortiz AR, Thomson P (2025) Multi-experimental seismic analysis of low-rise thin reinforced concrete wall building with unconnected elastomeric isolators using real-time hybrid simulations. Adv Struct Eng 28(2):372–90. https://doi.org/10.1177/13694332241281525
5. Castillo B, Vides SM, Marulanda J, Ortíz AR, Thomson P (2024) Seismic performance assessment of a low-rise thin reinforced concrete wall building with unconnected fiber reinforced elastomeric isolators using real-time hybrid simulations. J Build Eng 15:89
6. Chen P, Xu L, Xie X (2023) Enhanced design and experimental investigation of disc spring-based self-centering buckling-restrained braces with a compounded combination mode. Earthq Eng Struct Dyn 52(10)
7. Oviedo JA, DelPilar M (2006) Sistemas de control de respuesta sísmica en edificaciones. Rev EIA Número 6:105–120
8. Madera IE (2018) Desarrollo tecnológico de un aislador sísmico de bajo costo para edificaciones bajas. Universidad del Valle
9. Jones L, Anastasopoulos I (2023) Bearing capacity of breakwater subjected to tsunami-induced scour. J Geotechn Geoenviron Eng 149(6):04023032
10. Celebi M (2000) Design of seismic isolated structures: from theory to practice. Earthq Spectra16(3)
11. Chopra AK (2014) Dinámica de estructuras Vol. 4. J Chem Inf Model
12. Maddaloni G, Caterino N, Occhiuzzi A (2017) Shake table investigation of a structure isolated by recycled rubber devices and magnetorheological dampers. Struct Control Health Monit 24(5):e1906
13. Kim YS, Naik SP, Choi JH, Jin K, Ho GR, Kim T et al (2023) Kinematic analysis and fault-dependence of building-wall fracture patterns during moderate earthquakes. Geosci J27(6):769–780
14. Xu G, Guo T, Li A, Zhang H, Wang K, Xu J et al (2024) Seismic resilience enhancement for building structures: a comprehensive review and outlook. Structures 59
15. Lin Z, Xu L, Xie X (2024) Shape function-based multi-objective optimizations of seismic design of buildings with elastoplastic and self-centering components. Comput Struct 296:107303
16. Zhang H, Zhou X, Ke K, Yam MCH, He X, Li H (2023) Self-centring hybrid-steel-frames employing energy dissipation sequences: Insights and inelastic seismic demand model. J Build Eng 63:105451
17. Kelly JM (1999) The role of damping in seismic isolation. Earthq Eng Struct Dyn 28(1):3–20
18. Phillips BM, Spencer BF (2013) Model-based feedforward-feedback actuator control for real-time hybrid simulation. J Struct Eng 139(7):1205–1214

19. Lee Y, Kim H, Min S, Yoon H (2023) Structural damage detection using deep learning and FE model updating techniques. Sci Rep 13(1):18694
20. Cha YJ, Agrawal AK, Friedman A, Phillips B, Ahn R, Dong B et al (2014) Performance validations of semiactive controllers on large-scale moment-resisting frame equipped with 200-kN mr damper using real-time hybrid simulations. J Struct Eng 140(10):04014066
21. Zhu F, Wang JT, Jin F, Lu LQ (2017) Real-time hybrid simulation of full-scale tuned liquid column dampers to control multi-order modal responses of structures. Eng Struct 138:74–90
22. Yang TY, Mosqueda G, Stojadinovic B (2008) Evaluating the quality of hybrid simulation test using an energy-based approach. Beijing, China
23. Castillo B, Marulanda J, Thomson P Evaluation of the dynamic behavior of a building with thin reinforced concrete wall and non-connected isolators through real-time hybrid simulations [Internet]. Available from: https://www.researchgate.net/publication/362018531
24. Mosqueda G, Stojadinovic B, Mahin SA (2007) Real-time error monitoring for hybrid simulation. Part I: methodology and experimental verification. J Struct Eng 133(8):1100–1108
25. Phillips BM, Chae Y, Jiang Z, Spencer BF, Ricles JM, Christenson RE et al (2010) Real-time hybrid simulation benchmark study with a large-scale MR damper. In: 5th world conference on structural control and monitoring
26. Silva CE, Gomez D, Maghareh A, Dyke SJ, Spencer BF (2020) Benchmark control problem for real-time hybrid simulation. Mech Syst Signal Process 1:135
27. Ning X, Wang Z, Wu B (2020) Kalman filter-based adaptive delay compensation for benchmark problem in real-time hybrid simulation. Appl Sci (Switz) 10(20):7101
28. Tell S, Andersson A, Najafi A, Spencer BF, Karoumi R (2022) Real-time hybrid testing for efficiency assessment of magnetorheological dampers to mitigate train-induced vibrations in bridges. Int J Rail Transp 10(4):436–455
29. Li T, Su M, Sui Y, Ma L (2021) Real-time hybrid simulation on high strength steel frame with Y-shaped eccentric braces. Eng Struct 226:111369
30. Madera I (2018) Desarrollo tecnológico de un aislador sísmico de bajo costo para edificaciones bajas. [Cali, Colombia]: Tesis doctoral, Universidad del Valle
31. Naeim F, Kelly JM (1999) Design of seismic isolated structures: from theory to practice, 1st edn. Wiley, USA
32. Symans MD, Constantinou MC (1997) Seismic testing of a building structure with a semi-active fluid damper control system. Earthq Eng Struct Dyn 26(7):759–777
33. Luca SG, Pastia C (2009) Case study of variable orifice damper for seismic protection of stuctures. Politeh lasi Sect Construct Arhit 55:39
34. Ghaffarzadeh H, Dehrod EA, Talebian N (2013) Semi-active fuzzy control for seismic response reduction of building frames using variable orifice dampers subjected to near-fault earthquakes. JVC/J Vib Control 19(13):1980–1998
35. José T, Claribel Y (2024) Diseño e implementación de un sistema de control lineal cuadrático Gaussiano en un sistema no lineal electromecánico denominado Robot Balancín. Trabajo de Titulación, Universidad Estatal Peninsula de Santa Elena,ECUADOR
36. Bishop RC, Dorf RH (2011) Modern control system, 12th edn. Prentice Hall, USA
37. Nakata N, Laplace P, Song W, Chae Y, Marshall GA, Ou G, Song C (2014) Hybrid simulation: a discussion of current assessment measure. Indiana